Jahn-Teller driven quadrupolar ordering and spin-orbital dimer formation in GaNb$_4$Se$_8$

Tsung-Han Yang [1,*], Tieyan Chang,[2] Yu-Sheng Chen,[2] and K. W. Plumb [1,†]

[1]*Department of Physics, Brown University, Providence, Rhode Island 02912, USA*
[2]*NSFs ChemMatCARS, the University of Chicago, Lemont, Illinois 60439, USA*

The lacunar spinel GaNb$_4$Se$_8$ is a tetrahedral cluster Mott insulator where spin-orbit coupling on molecular orbitals and Jahn-Teller energy scales are competitive. GaNb$_4$Se$_8$ undergoes a structural and antipolar ordering transition at T$_Q$ = 50 K that corresponds to a quadrupolar ordering of molecular orbitals on Nb$_4$ clusters. A second transition occurs at T$_M$ = 29 K, where local distortions on the Nb$_4$ clusters rearrange. We present a single crystal x-ray diffraction investigation for these phase transitions and solve the crystal structure in the intermediate $T_M < T < T_Q$ and low $T < T_M$ temperature phases. The intermediate phase is a primitive cubic P2$_1$3 structure with a staggered arrangement of Nb$_4$ cluster distortions. A symmetry mode analysis reveals that the transition at T$_Q$ is continuous and described by a single Jahn-Teller active distortion mode. In the low temperature phase, the symmetry of Nb$_4$ clusters is further reduced and a staggered arrangement of intercluster dimers is formed, suggesting a valence bond solid magnetic state.

I. INTRODUCTION

The many interesting properties of strongly correlated magnetic materials arise from an interplay of charge, spin, orbital, and lattice degrees of freedom. In transition metal materials, it is often the case that spin and orbital effects appear in a hierarchy of well separated energy scales and can be considered to act independently of each other. For example, in transition metal materials that have an orbital degeneracy, the orbital degrees of freedom are typically quenched out via a Jahn-Teller mechanism at a high temperature relative to the magnetic ordering temperatures, rendering a spin only magnetic model. However, for $4d$ or $5d$ transition metal materials, relativistic spin-orbit coupling can significantly alter this energy hierarchy, giving rise to magnetic phases with spin-orbital entangled degrees of freedom. The presence of such spin-orbital degrees of freedom dramatically influences magnetic ground states and are the essential microscopic ingredient to stabilize, for example, Kitaev spin liquids, topological superconductors, or spin-orbital liquid phases depending on the particular electron filling [1–5]. In particular, $4d^1$ or $5d^1$ Mott insulators with a single electron occupying the $j = 3/2$ spin-orbital state have attracted significant attention [3,6–9] as materials where multipolar orders or spin-orbital liquids may be realized. Lacunar spinels with the chemical formula GaM_4X_8 (M = V, Nb, Ta; X = S, Se) are a family of cluster Mott insulators that contain a single unpaired electron occupying molecular t_2 orbitals on each M$_4$ cluster site [Fig. 1(a)] [10,11]. The isostructural members of this family that contain 3d, 4d, and 5d transition metals

respectively provide an ideal opportunity to investigate the interplay of spin, orbit, and lattice degrees of freedom as atomic spin-orbit coupling and correlations are systematically varied. Indeed, clear trends in the relative separation of spin and orbital energy scales are observed across the series. In GaV$_4$S$_8$ and GaV$_4$Se$_8$ the orbital degrees of freedom are quenched through a high temperature Jahn-Teller (JT) distortion that is preceded by spin ordering at lower temperatures [12,13]. The JT distortion generates an electric dipole moment on each V$_4$ cluster that is oriented uniformly along the same direction for each cluster resulting in a ferropolar ordering [14–18]. On the other hand, in those compounds where spin-orbit coupling is the strongest, GaNb$_4$S$_8$ and GaTa$_4$Se$_8$, there is only a single magnetostructural transition leading to a dimerized, valence bond solid, ground state [19,20]. The single transition, simultaneously involving spin and orbital degrees of freedom implies a vanishing separation between spin and orbital energy scales. Indeed, in GaTa$_4$Se$_8$, the correlated units are molecular spin-orbit entangled $j_{eff} = 3/2$ [10,21–23] degrees of freedom. In such a spin-orbital state, JT effects are suppressed, but substantial spin-orbital dynamics are reflected in the disorder-order nature of the spin-orbital transition and corresponding phonon anomaly above the transition [22]. The structural distortions in GaNb$_4$S$_8$ and GaTa$_4$Se$_8$ also generate electric dipoles on the transition metal clusters, but in these materials the distortions arrange in a staggered or antiferropolar ordering [17,22,24,25].

GaNb$_4$Se$_8$ presents an interesting intermediate regime where spin-orbit coupling and JT energy scales are on a more equal footing. In this material, there is a cubic-to-cubic structural phase transition at T$_Q$ = 50 K preceding a magnetostructural distortion [20,25,26] and the formation of structural dimers at T$_M$ = 29 K, illustrated in Fig. 1. The cubic-to-cubic structural distortion is associated with an anomaly in the temperature dependent dielectric constant [25]

---

*Present address: Neutron Scattering Division, Oak Ridge National Laboratory, Oak Ridge, TN 37831, USA.
†Corresponding author: kemp_plumb@brown.edu

144101-1
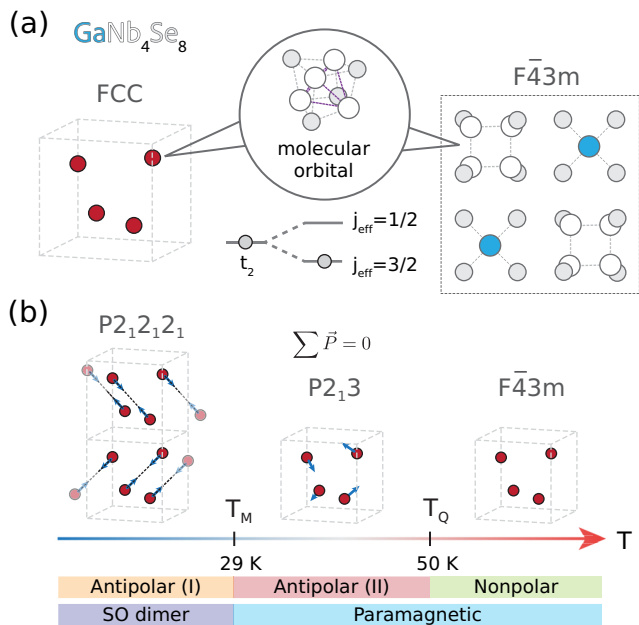
FIG. 1. (a) Crystal structure and molecular orbital level scheme GaNb$_4$Se$_8$. The correlated units are molecular $j_{\text{eff}} = 3/2$ orbitals on Nb$_4$Se$_4$ cubane units. Each Nb$_4$ cluster occupies an FCC lattice site. (b) Structural, magnetic, and polar phases transitions in GaNb$_4$Se$_8$ at different temperatures. The total polarization for two antipolar phases are zero while the internal arrangements differ.

and the intermediate state suggests the possibility for antiferroelectric quadrupolar ordering of $j = 3/2$ spin-orbital degrees of freedom [20]. An additional anomaly of the dielectric constant at T$_M$ suggests a second rearrangement of electric quadrupoles at this temperature [25]. However, the precise form of quadrupolar ordering and underlying mechanisms in GaNb$_4$Se$_8$ have not been resolved because the crystal structures and atomic positions associated with the phases for T$_M$ < T < T$_Q$ and T < T$_M$ are not known. This difficulty arises because of weak diffraction intensities from low temperature superlattice structural peaks, hindering the refinement of powder diffraction measurements, and from complications from domains in the low temperature orthorhombic unit cell. Detailed knowledge of the crystal structure, and especially the transition metal atomic positions, is essential to resolve the nature of quadrupolar or orbital ordering in this material and elucidate the microscopic mechanism driving this phenomena.

In this work, we investigate the temperature-dependent crystal structure of GaNb$_4$Se$_8$ using synchrotron single crystal x-ray diffraction. We determine the intermediate T$_M$ < T < T$_Q$ and low temperature T < T$_M$ crystal structures of GaNb$_4$Se$_8$ and find that the intermediate cubic structure is consistent with previous reports [20]. However, a full refinement of the structure enables a symmetry analysis of the structural transition at T$_Q$. This analysis reveals it to be a continuous (second order) transition described by a single JT active distortion of Nb$_4$ clusters. At T$_M$ = 29 K, GaNb$_4$Se$_8$ further undergoes a first order cubic to orthorhombic transition. The unit cell doubles through this transition as Nb$_4$ clusters rearrange to form structural dimers along

cubic ⟨011⟩ directions, consistent with the development of a correlated singlet, or valence bond solid state, that is similar to GaTa$_4$Se$_8$ [22]. Our work sheds light on the complex interplay between spin-orbit coupling, lattice distortions, and intercluster interactions to effect electric quadrupolar orderings in lacunar spinels and provides essential crystal structure information to support further investigation of spin-orbital physics in molecular Mott insulators.

II. METHODS

A. Sample synthesis

Polycrystalline samples of GaNb$_4$Se$_8$ were synthesized by solid-state reaction. About 1.5 g of stoichiometric quantities of high-purity raw materials (Gallium: Alfa Aesar, 99.999%; Niobium: Alfa Aesar, 99.99%; Selenium: Alfa Aesar, 99.999%) were loaded into I.D. = 10 mm, 100 mm long quartz ampules under an argon glovebox. The ampules were evacuated, and sealed before heating to 1050 °C with 80 °C/hour ramping rate, held for 24 hours and then air quenched to room temperature. The resulting powder was reground in an argon glovebox, resealed under vacuum, and heated following the same procedure. Three heating and regrinding repetitions were required to obtain single-phase polycrystalline samples. The composition was confirmed by powder x-ray diffraction (Bruker Cu Kα radiation). Micron scale single crystals of GaNb$_4$Se$_8$ were prepared by chemical vapor transport from the phase pure powders. About 1.5 g of single-phase GaNb$_4$Se$_8$ powder and 75 mg iodine were sealed in I.D. =10 mm, 210 mm long quartz ampules. The ampule was placed in a two-zone furnace with 950 °C and 1000 °C zone temperatures for 20 days.

B. X-ray crystallography

Temperature dependent x-ray diffraction was carried out using a four-circle x-ray diffractometer, and Ag Kα radiation, with an XSpectrum Lambda 60 K GaAs photon counting detector positioned 78 cm from the sample. The single crystal sample was mounted in reflection geometry on a Cu post on the coldfinger of a closed cycle cryostat for measurements between 3 and 300 K.

Synchrotron crystallography measurements were performed on the 15 ID-D beamline at the Advanced Photon Source at Argonne National Laboratory. The sample was mounted on a quartz fiber with epoxy adhesive. We used a 30 keV x-ray beam and Dectris Pilatus3X 1M CdTe area detector with a sample to detector distance of 130 mm for 100 K and 120 mm for 40 K and 20 K measurements. Nitrogen and helium cryostreams were used to control the sample temperature. For each temperature, diffraction images were collected by rotating the sample through 360 degrees with 0.3 degrees/step for 100 K measurements and 0.1 degrees/step for 40 K and 20 K measurements. The images were integrated into reciprocal space and indexed using BRUKER APEX4 software. Absorption corrections were applied using SADABS and TWINABS packages, and the space group was checked using the XPREP package. The final crystal structure solution and refinements were performed on SHELX with the OLEX2 user interface [27,28].
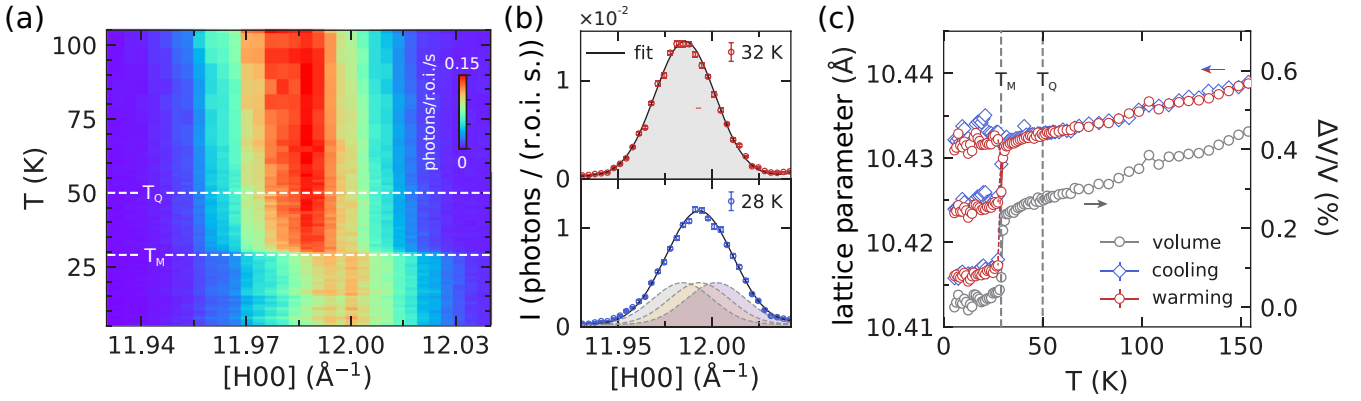
FIG. 2. (a) Temperature-dependent single crystal x-ray diffraction of the cubic [12, 0, 0] Bragg reflection in $GaNb_4Se_8$. The [12, 0, 0] reflection is not sensitive to the transition at T_Q but displays a clear shift and broadening below T_M in the orthorhombic cell phase. (b) Gaussian fits of the [12, 0, 0] reflection above and below T_M. The peak width is fixed to instrumental resolution for the fit below T_M. (c) Temperature dependent lattice parameter(s) and the cell volume extracted from [12, 0, 0] reflection.

III. RESULTS

A. Jahn-Teller driven antiferroquadrupolar order

We first investigate the structural phase transition at $T_Q = 50$ K. Temperature-dependent diffraction measurements of a cubic [12, 0, 0] Bragg peak are shown in Fig. 2. The cubic peak exhibits noticeable broadening at $T_M = 29$ K, but no detectable change across T_Q [Fig. 2(a)], consistent with a cubic-cubic phase transition. The temperature dependent lattice parameters and cell volume extracted from Gaussian fits of a longitudinal cut through the [12, 0, 0] peak are shown in Fig. 2(c), demonstrating a continuous variation across T_Q, consistent with the second order nature of this transition.

Synchrotron x-ray crystallography at 40 K reveals a primitive cubic unit cell and space group $P2_13$. Figure 3 shows the appearance of reflections for $h + k = 2n$, $h + l = 2n$, and $k + l = 2n$ that violate reflection conditions for a face-center-cubic (FCC) cell and indicate a primitive cubic unit cell at 40 K. Our refinement gives the best fit to the $P2_13$ space group with $R_1 = 0.0442$ ($I \geqslant 2\sigma$). Nb atoms sit on $16e$ Wyckoff positions (WP) in the high temperature cubic phases that split into $4a$ and $12b$ WPs in the $P2_13$ structure resulting in an elongation of Nb_4 tetrahedra along the cubic $\langle \bar{1}11 \rangle$ directions as shown in Figs. 5(a) and 5(b). Parameters of the refinement are listed in Table III and the refined atomic positions are listed in the Supplemental Material [29]. The space group and refined structure exhibiting a staggered arrangement of Nb_4 cluster distortions are consistent with antiferroquadrupolar ordering previously proposed in this regime [20,25].

We find that the transition at T_Q is second order, consistent with the absence of any detectable volume change or hysteresis through the transition [Fig. 2(c)], and a single irreducible representation order parameter for the distortion. The second order nature is apparent in Fig. 4, and shows the continuous onset of the [8, 0, 1] reflection intensity at T_Q. This Bragg reflection is directly related to a single amplitude mode order parameter [Fig. 5(b)] identified for this structural transition.

A symmetry mode analysis through the cubic-cubic $F\bar{4}3m \rightarrow P2_13$ distortion was carried out using the Bilbao crystallographic server [30–32] to yield the primary mode amplitudes and isotrophy space groups listed in Table I.

Corresponding atomic distortions for each symmetry mode are listed in Supplemental Material [29]. The structural transition at T_Q is described by two primary distortions: Γ_1, which belongs to $F\bar{4}3m$, and a dominant JT active X_5 mode that belongs to $P2_13$ and acts to distort Nb_4 clusters along $\langle \bar{1}11 \rangle$ directions, as shown in Figs. 5(a) and 5(b). This second-order transition at T_Q can be naturally described as a continuous increase of the X_5 mode amplitude order parameter [Fig. 5(b)] that leads to the development of quadrupolar moments on Nb_4 clusters. Thus, a JT distortion of Nb_4 clusters underlies staggered quadrupolar ordering at T_Q in $GaNb_4Se_8$, similar to the proposed JT mechanism driving antipolar order in
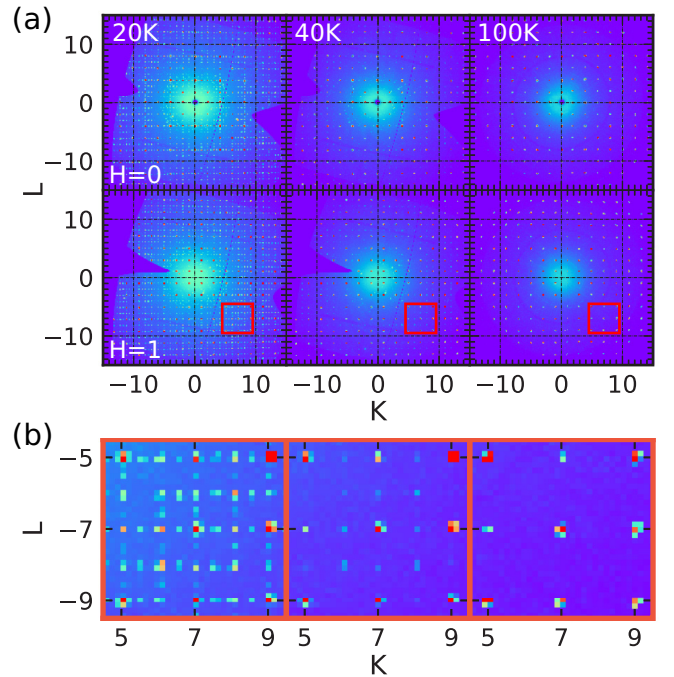
FIG. 3. (a) Reconstruction of (0KL) and (1KL) planes in reciprocal space from x-ray crystallography at 20, 40, and 100 K. (b) Zoomed areas in (1KL) plane, indicated by red boxes in (a), demonstrate the appearance of superlattice reflections.
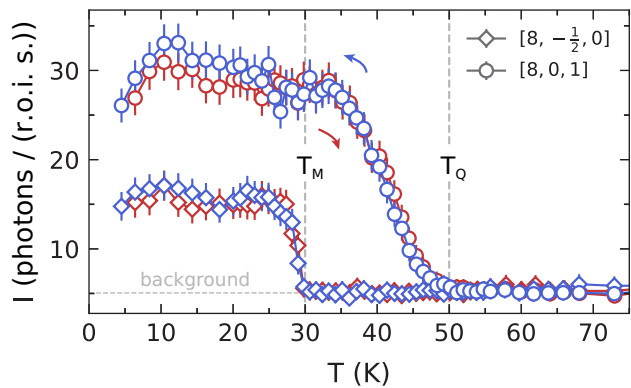
FIG. 4. Temperature-dependent peak intensities of $[8, 0, 1]$ Bragg peak that represents the order parameter for the F$\bar{4}$3m to P2$_1$3 structural transition at T$_Q$ = 50 K, and $[8, -\frac{1}{2}, 0]$ reflection that shows a unit cell doubling through the first order transition at T$_M$ = 29 K. The background level is calculated by averaging the counts of a r.o.i. away from Bragg peaks above 60 K.

GaNb$_4$S$_8$ [17]. However, it is interesting that in GaNb$_4$Se$_8$ the transition at T$_Q$ solely involves the ordering of structural (orbital) degrees of freedom, while magnetic and structural degrees of freedom undergo a second simultaneous transition at lower temperatures T$_M$ < T$_Q$. This separation of energy scales is distinct from GaNb$_4$S$_8$ and GaTa$_4$Se$_8$ where there is only a single transition involving the structural and magnetic degrees of freedom.

B. Structural dimers in the antipolar I ordered phase

We now examine the evolution of the crystal structure through the first-order phase transition at T$_M$ = 29 K, where a simultaneous structural transition and reduction in the temperature dependent magnetization occur. As shown in Fig. 3 and Fig. 4, superlattice Bragg reflections, at $[\frac{1}{2}, 0, 0]$ positions of the cubic cell, appear upon cooling below T$_M$. These indicate a unit cell doubling along one axis through a cubic to orthorhombic structural transition, similar to what has been observed in GaNb$_4$S$_8$ [17] and GaTa$_4$Se$_8$ [22]. The first order nature of this transition is identified though a discontinuous change in lattice parameters and cell volume [Fig. 2(c)], a discontinuous onset of supperlattice reflection intensity [Fig. 4], and sharp, divergent, heat capacity [25].

In order to account for the formation of structural domains through this transition, we define four twinned cells for each doubled axis along the crystallographic a, b, or c axis by rotating against the doubled axis through 0, 90, 180, and 270 degrees, giving 12 domains in total. Integrated intensities of Bragg reflections were corrected based on symmetry

TABLE I. Irreducible representation of distortion modes for F$\bar{4}$3m to P2$_1$3 transition, amplitudes are normalized to the primitive unit cell of the high-symmetry F$\bar{4}$3m structure.

$\vec{K}$	Irrep	Direction	Isotropy SG	Amp. (Å)
(0,0,0)	Γ_1	(a)	F$\bar{4}$3m	0.0037
(0,1,0)	X_5	(a,a,a,a,a,a)	P2$_1$3	0.0826
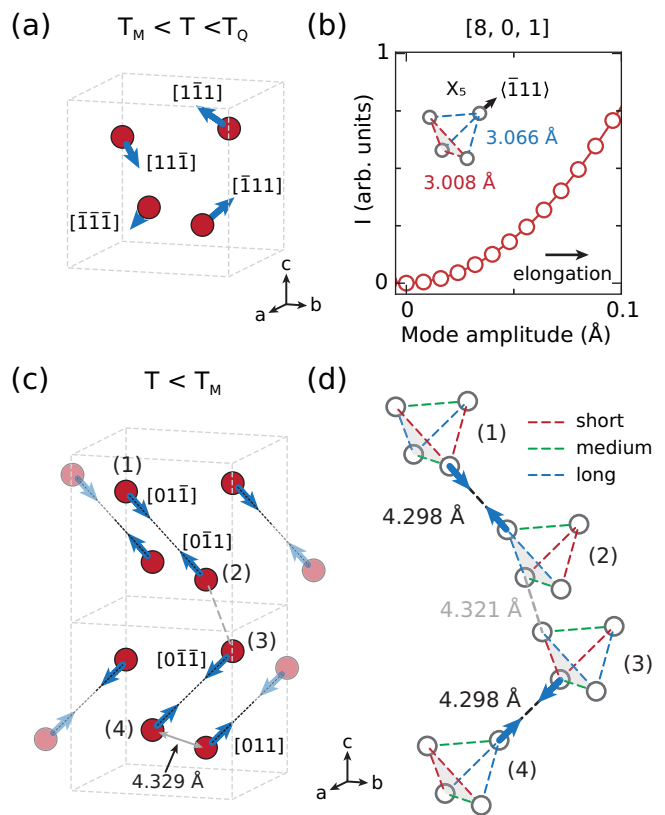
FIG. 5. (a) Schematic representation of Nb$_4$ tetrahedron distortions in the T = 40 K refined crystal structure. Red circles represent Nb$_4$ clusters, and blue arrows indicate the direction of overall distortion on each cluster in the cubic cell. (b) Simulated $[8,0,1]$ peak intensity (using DANS DIFFRACTION package [33]) and distortion on each Nb$_4$ cluster. The intensity of a $[8,0,1]$ structural Bragg peak continuously increases with the X_5 distortion, as Nb$_4$ clusters elongate along $\langle\bar{1}11\rangle$ directions of the cubic P2$_1$3 cell. (c) Schematic of Nb$_4$ cluster distortions in the orthorhombic P2$_1$2$_1$2$_1$ cell at 20 K. Black dashed lines indicate the closest distance between neighboring clusters, showing a dimerized structure. (d) Schematic of the distortion of Nb$_4$ clusters. The location of each cluster within the orthorhombic cell are labeled with corresponding numbers in (c). Each cluster has two long bonds (blue), two short bonds (red), and two intermediate bonds (green).

operations using TWINABS for these 12 domains. The observation of reflections at $h + k + l \neq 2n$ and $h + k \neq 2n$ rule out most of the orthorhombic space groups, excepting P222, P222$_1$, P2$_1$2$_1$2, and P2$_1$2$_1$2$_1$. After accounting for the domain structure and reflection conditions, our crystallographic refinement gives the best agreement with a unit cell doubled orthorhombic P2$_1$2$_1$2$_1$ space group with R_1 = 0.0855 ($I \geqslant 2\sigma$). Refinement parameters are listed in Table III, and the refined structure is shown in Figs. 5(c) and 5(d).

Figures 5(c) and 5(d) show the refined crystal structure and refined atomic positions are listed in the Supplemental Material [29]. At T$_M$, Nb$_4$ clusters distort so that each tetrahedron elongates along cubic $\langle 011 \rangle$ or equivalent directions [Fig. 5(c)] and has three inequivalent bond lengths as illustrated in Fig. 5(d). Distorted Nb$_4$ tetrahedra rearrange so that each points toward a single neighboring cluster, forming

TABLE II. Irreducible representation of distortion modes for $F\bar{4}3m$ to $P2_12_12_1$ transition, amplitudes are normalized to the primitive unit cell of the high-symmetry $F\bar{4}3m$ structure.

$\vec{K}$	Irrep	Direction	Isotropy SG	Amp. (Å)
(0,0,0)	Γ_1	(a)	$F\bar{4}3m$	0.0045
(0,0,0)	Γ_3	(a,b)	$F222$	0.0035
$(0,\frac{1}{2},0)$	$\Delta_3\Delta_4$	(0,0,0,0,a,b,0,0,0,0,-b,a)	$C222_1$	0.0697
(0,1,0)	X_3	(0,a,0)	$P\bar{4}m2$	0.0294
(0,1,0)	X_4	(0,a,0)	$P\bar{4}n2$	0.0042
(0,1,0)	X_5	(0,0,a,b,0,0)	$P2_12_12$	0.1140
$(\frac{1}{2},1,0)$	W_1	(0,0,0,0,-a,a)	$I\bar{4}2d$	0.0202
$(\frac{1}{2},1,0)$	W_2	(0,0,0,0,-a,a)	$I\bar{4}2d$	0.0295

structural dimers along $\langle 011 \rangle$ or $\langle 0\bar{1}1 \rangle$ directions as indicated in Fig. 5(c). The symmetry reduction on Nb$_4$ tetrahedra must have an associated reorientation of the polar axis, and their staggered arrangement indicates an antipolar ordering. Thus, the crystal structures reported here are consistent with the two successive antipolar orderings found at T$_Q$ and T$_M$ in GaNb$_4$Se$_8$ [25], and reveal the nature of those orderings. The structural dimer motif and vanishing magnetization at T$_M$ [20,25] also suggest that magnetic singlets form across intercluster dimers as GaNb$_4$Se$_8$ enters a valence bond crystallike state below T$_M$, similar to what has been observed in GaTa$_4$Se$_8$ [22].

The unit cell doubled P2$_1$2$_1$2$_1$ structure is not a subgroup of the intermediate P2$_1$3 structure, and the transition at T$_M$ cannot be described with a JT active mode as for that at T$_Q$. The $1 \times 1 \times 1$ orthorhombic P2$_1$2$_1$2$_1$ is the exclusive subgroup of the intermediate P2$_1$3 structure, while the superlattice reflections indicate the structure is a $1 \times 1 \times 2$ cell [Fig. 3]. Therefore, in order to better interrogate the mechanisms that underlie this transition, we compute structure relations against the high temperature F$\bar{4}$3m structure to obtain irreducible representations and distortion mode amplitudes listed in Table II. The distortion again involves a JT active X_5 mode that generates the intermediate cubic phase, but there are also other unit cell doubling distortions of comparable magnitude that modulate Se positions and intercluster bonds and mix with the JT active modes. The necessity of multiple distortion modes to describe the transition at T$_M$ is consistent with the involvement of more than one order parameter, including at least structural and magnetic degrees of freedom, and indicates that a simple JT mechanism is not the origin of the transition at T$_M$. An involvement of distortions that modulate intercluster bonds, and the formation of magnetic singlets, indicates that the transition at T$_M$ may instead be driven by intercluster interactions, similar to GaTa$_4$Se$_8$ [22].

IV. DISCUSSION

It is instructive to compare the phase transitions in other isostructural and isoelectronic lacunar spinels. The particular sequence of phase transitions with decreasing temperature, and low-temperature crystal structures of GaM_4X$_8$ (M = V, Nb, Ta; X = S, Se) are set by an interplay between JT effects, that act to quench orbital momentum, and spin-orbit coupling on the molecular orbitals, that acts to maintain an

orbital character. When the JT effect dominates (M = V), the orbital and magnetic sectors are distinct, i.e., a high temperature JT structural transition quenches the orbital degrees of freedom and is preceded by spin ordering at a lower temperature [12,14,34,35]. In both GaV$_4$S$_8$ and GaV$_4$Se$_8$, the JT distortion selects a ferropolar order with a charge dipole directed along cubic $\langle 111 \rangle$ directions [14,35]. In the opposite limit of dominant spin-orbit coupling, as is relevant for GaTa$_4$Se$_8$, the spin and orbital energy scales are not separate and the relevant degrees of freedom are spin-orbital entangled $j_{\rm eff} = 3/2$ states [21,23]. In this case, there is a single magnetostructural transition at T$^* = 50$ K that cannot be described by a JT active mode [22]. Below T*, GaTa$_4$Se$_8$ enters a valence bond-solid-like ground state, and the transition at T* is driven by interactions between Ta$_4$ clusters [22] that sets up a staggered arrangement of cluster distortions.

GaNb$_4$S$_8$ and GaNb$_4$Se$_8$ sit at an intermediate spin-orbit coupling strength, where the interplay between SOC and the JTE becomes most apparent. Since electrons occupy molecular orbitals on cubane (M_4X_4; M = V, Nb, Ta; X = S, Se) units in the lacunar spinels, the effective molecular spin-orbit coupling is the relevant energy scale. Molecular orbitals are formed from a linear combination of atomic d orbitals, so the effective spin-orbit coupling strength will increase with increasing transition metal atomic number, but decrease as the M-X orbital hybridization and effective size of molecular orbitals is increased. Thus, the effective spin-orbit coupling strength should be larger in GaNb$_4$S$_8$ compared with GaNb$_4$Se$_8$ because the broader spatial extent of Se orbitals will enhance M-X hybridization across cubane units. This expectation is borne out through the appearance of only a single transition involving the magnetic and structural degrees of freedom in GaNb$_4$S$_8$, but a separation of energy scales and two transitions in GaNb$_4$Se$_8$. However, unlike the Vanadium compounds, both transitions in GaNb$_4$Se$_8$, at T$_Q$ and T$_M$, involve rearrangements of Nb$_4$ clusters and an associated change in the molecular orbital configuration. In other words, the JT transition at T$_Q$ does not act to quench orbital degrees of freedom but instead reduces degeneracy by imposing a staggered quadrupolar order involving spin-orbital moments. As previously pointed out [20], such a transition is similar to the expected quadrupolar ordering predicted for $j = 3/2$ double perovskites [6]; however, we find that quadrupolar ordering in GaNb$_4$Se$_8$ predominantly involves a JT mechanism (ionic motion), and does not require an intersite orbital exchange, although our data does not rule out such an interaction.

The JT transition involving spin-orbital degrees of freedom favors an antipolar order in GaNb$_4$Se$_8$ [25], with the staggered polar vector oriented along $\langle 111 \rangle$ directions, rather than $\langle 111 \rangle$ ferropolar order as in GaV$_4$S$_8$ and GaV$_4$Se$_8$ [35]. At lower temperatures, a non-JT mechanism results in a rearrangement of the Nb$_4$ clusters to orient staggered polar order along $\langle 110 \rangle$ directions and form structural dimers. This second transition is similar to the spin-orbital ordering transition at T* in GaTa$_4$Se$_8$ in that it involves distortions that strongly modulate intercluster bonds and Se positions, and results in an intercluster structural dimerization along $\langle 110 \rangle$ directions. Although the particular staggered pattern of dimers is different between these two compounds, it is likely that both the transition at T*

TABLE III. Crystallographic refinement results at 20, 40, and 100 K.

Temperature (K)	20	40	100
Crystal system	orthorhombic	cubic	cubic
Space group	$P2_12_12_1$	$P2_13$	$F\bar{4}3m$
a (Å)	10.4090(5)	10.4071(6)	10.40910(10)
b (Å)	10.4086(5)		
c (Å)	20.8145(10)		
Data collection diffractometer	15-ID-D, APS	15-ID-D, APS	15-ID-D, APS
Absorption correction	Multiscan	Multiscan	Multiscan
Reflections collected	66929	17258	13368
Independent reflections	16630 ($R_{int} = 0.0422$)	2489 ($R_{int} = 0.0273$)	464 ($R_{int} = 0.0340$)
F(000)	3736.0	1401.0	1868.0
λ (Å, synchrotron)	0.41328	0.41328	0.41328
2θ range for data collection (deg)	2.544 to 50.64	3.218 to 49.048	3.94 to 47.77
Index ranges	$-18 \leqslant h \leqslant 19$	$-18 \leqslant h \leqslant 18$	$-17 \leqslant h \leqslant 15$
	$-19 \leqslant k \leqslant 19$	$-13 \leqslant k \leqslant 16$	$-19 \leqslant k \leqslant 17$
	$-38 \leqslant l \leqslant 38$	$-15 \leqslant l \leqslant 18$	$-17 \leqslant l \leqslant 19$
Data, restraints, parameters	16630/0/205	2489/0/41	464/0/12
Goodness of fit	1.088	1.272	1.190
R_1, $wR_2 (I \geqslant 2\sigma)$	0.0855, 0.1777	0.0442, 0.0776	0.0088, 0.0200
R_1, wR_2(all)	0.0910, 0.1794	0.0470, 0.0789	0.0088, 0.0200
Largest diff. peak/hole	8.10/−7.15	4.92/−2.54	0.98/−0.96

in $GaTa_4Se_8$ and at T_M in $GaNb_4Se_8$ are driven by intercluster spin-orbital interactions.

V. SUMMARY AND CONCLUSIONS

We have solved crystal structures of $GaNb_4Se_8$ in the intermediate $T_M < T < T_Q$ and low $T < T_M$ temperature regimes and find that the transitions at T_Q and T_M involve distinct mechanisms. At T_Q, we find a continuous second-order Jahn-Teller, quadrupolar ordering, phase transition on a Nb_4 tetrahedron. At $T < T_M$, the unit cell doubles along one axis and forms a singlet dimer state, resembling the sibling compound $GaTa_4Se_8$ [22]. Compared to previous studies on heat capacity, magnetic susceptibility, and dielectric measurements [20,25], our results complete the thus far missing structural information for $GaNb_4Se_8$. By identifying the structural mechanisms of staggered quadrupolar orderings, these results provide insights into material parameters controlling polar ordering in the orbitally degenerate lacunar spinels. In

the future it would be interesting to directly interrogate the spin-and-orbital dynamics in these materials and explore how these energy scales relate to the high pressure superconducting phases in $GaTa_4Se_8$ and $GaNb_4S_8$ [4,26,36,37].

[1] W. Witczak-Krempa, G. Chen, Y. Baek Kim, and L. Balents, Correlated quantum phenomena in the strong spin-orbit regime, Annu. Rev. Condens. Matter Phys. **5**, 57 (2014).

[2] K. W. Plumb, J. P. Clancy, L. J. Sandilands, V. Vijay Shankar, Y. F. Hu, K. S. Burch, H.-Y. Kee, and Y.-J. Kim, α-RuCl$_3$: A spin-orbit assisted Mott insulator on a honeycomb lattice, Phys. Rev. B **90**, 041112(R) (2014).

[3] J. Romhányi, L. Balents, and G. Jackeli, Spin-orbit dimers and noncollinear phases in d^1 cubic double perovskites, Phys. Rev. Lett. **118**, 217202 (2017).

[4] M. J. Park, G. Sim, M. Y. Jeong, A. Mishra, M. J. Han, and S. Lee, Pressure-induced topological superconductivity in the spin-orbit Mott insulator $GaTa_4Se_8$, npj Quantum Mater. **5**, 41 (2020).

[5] N. Tang, Y. Gritsenko, K. Kimura, S. Bhattacharjee, A. Sakai, M. Fu, H. Takeda, H. Man, K. Sugawara, Y. Matsumoto, Y. Shimura, J. Wen, C. Broholm, H. Sawa, M. Takigawa, T. Sakakibara, S. Zherlitsyn, J. Wosnitza, R. Moessner, and S. Nakatsuji, Spin–orbital liquid state and liquid–gas metamagnetic transition on a pyrochlore lattice, Nat. Phys. **19**, 92 (2023).

[6] G. Chen, R. Pereira, and L. Balents, Exotic phases induced by strong spin-orbit coupling in ordered double perovskites, Phys. Rev. B **82**, 174440 (2010).

[7] W. M. H. Natori, E. C. Andrade, E. Miranda, and R. G. Pereira, Chiral spin-orbital liquids with nodal lines, Phys. Rev. Lett. **117**, 017204 (2016).

[8] N. Iwahara, V. Vieru, and L. F. Chibotaru, Spin-orbital-lattice entangled states in cubic d^1 double perovskites, Phys. Rev. B **98**, 075138 (2018).

[9] W. M. H. Natori, M. Daghofer, and R. G. Pereira, Dynamics of a $j = 3/2$ quantum spin liquid, Phys. Rev. B **96**, 125109 (2017).

[10] H.-S. Kim, J. Im, M. Joon Han, and H. Jin, Spin-orbital entangled molecular j_{eff} states in lacunar spinel compounds, Nat. Commun. **5**, 3988 (2014).

[11] H.-S. Kim, K. Haule, and D. Vanderbilt, Molecular Mott state in the deficient spinel GaV_4S_8, Phys. Rev. B **102**, 081105(R) (2020).

[12] R. Pocha, D. Johrendt, and R. Pöttgen, Electronic and structural instabilities in GaV_4S_8 and $GaMo_4S_8$, Chem. Mater. **12**, 2882 (2000).

[13] Z. Wang, E. Ruff, M. Schmidt, V. Tsurkan, I. Kézsmárki, P. Lunkenheimer, and A. Loidl, Polar dynamics at the Jahn-Teller transition in ferroelectric GaV_4S_8, Phys. Rev. Lett. **115**, 207601 (2015).

[14] E. Ruff, A. Butykai, K. Geirhos, S. Widmann, V. Tsurkan, E. Stefanet, I. Kézsmárki, A. Loidl, and P. Lunkenheimer, Polar and magnetic order in GaV_4Se_8, Phys. Rev. B **96**, 165119 (2017).

[15] Á. Butykai, S. Bordács, I. Kézsmárki, V. Tsurkan, A. Loidl, J. Döring, E. Neuber, P. Milde, S. C. Kehr, and L. M. Eng, Characteristics of ferroelectric-ferroelastic domains in Néel-type skyrmion host GaV_4S_8, Sci. Rep. **7**, 44663 (2017).

[16] K. Geirhos, B. Gross, B. G. Szigeti, A. Mehlin, S. Philipp, J. S. White, R. Cubitt, S. Widmann, S. Ghara, P. Lunkenheimer, V. Tsurkan, E. Neuber, D. Ivaneyko, P. Milde, L. M. Eng, A. O. Leonov, S. Bordács, M. Poggio, and I. Kézsmárki, Macroscopic manifestation of domain-wall magnetism and magnetoelectric effect in a Néel-type skyrmion host, npj Quantum Mater. **5**, 44 (2020).

[17] K. Geirhos, J. Langmann, L. Prodan, A. A. Tsirlin, A. Missiul, G. Eickerling, A. Jesche, V. Tsurkan, P. Lunkenheimer, W. Scherer, and I. Kézsmárki, Cooperative Cluster Jahn-Teller effect as a possible route to antiferroelectricity, Phys. Rev. Lett. **126**, 187601 (2021).

[18] S. Ghara, K. Geirhos, L. Kuerten, P. Lunkenheimer, V. Tsurkan, M. Fiebig, and I. Kézsmárki, Giant conductivity of mobile non-oxide domain walls, Nat. Commun. **12**, 3975 (2021).

[19] O. Arnold, J. C. Bilheux, J. M. Borreguero, A. Buts, S. I. Campbell, L. Chapon, M. Doucet, N. Draper, R. Ferraz Leal, M. A. Gigg, V. E. Lynch, A. Markvardsen, D. J. Mikkelson, R. L. Mikkelson, R. Miller, K. Palmen, P. Parker, G. Passos, T. G. Perring, P. F. Peterson *et al.*, Mantid Data analysis and visualization package for neutron scattering and μSR experiments, Nucl. Instrum. Methods Phys. Res. Sect. A **764**, 156 (2014).

[20] H. Ishikawa, T. Yajima, A. Matsuo, Y. Ihara, and K. Kindo, Nonmagnetic ground states and a possible quadrupolar phase in $4d$ and $5d$ lacunar spinel selenides GaM_4Se_8 (M = Nb, Ta), Phys. Rev. Lett. **124**, 227202 (2020).

[21] M. Y. Jeong, S. H. Chang, B. H. Kim, J.-H. Sim, A. Said, D. Casa, T. Gog, E. Janod, L. Cario, S. Yunoki, M. Joon Han, and J. Kim, Direct experimental observation of the molecular $J_{eff} = 3/2$ ground state in the lacunar spinel $GaTa_4Se_8$, Nat. Commun. **8**, 782 (2017).

[22] T.-H. Yang, S. Kawamoto, T. Higo, S. G. Wang, M. B. Stone, J. Neuefeind, J. P. C. Ruff, A. M. M. Abeykoon, Y.-S. Chen, S. Nakatsuji, and K. W. Plumb, Bond ordering and molecular spin-orbital fluctuations in the cluster Mott insulator $GaTa_4Se_8$, Phys. Rev. Res. **4**, 033123 (2022).

[23] T. Petersen, P. Bhattacharyya, U. K Rößler, and L. Hozoi, Resonating holes vs molecular spin-orbit coupled states in group-5 lacunar spinels, Nat. Commun. **14**, 5218 (2023).

[24] S. Jakob, H. Müller, D. Johrendt, S. Altmannshofer, W. Scherer, S. Rayaprol, and R. Pöttgen, Structural and magnetic transitions in the Mott insulator $GaNb_4S_8$, J. Mater. Chem. **17**, 3833 (2007).

[25] M. Winkler, L. Prodan, V. Tsurkan, P. Lunkenheimer, and I. Kézsmárki, Antipolar transitions in $GaNb_4Se_8$ and $GaTa_4Se_8$, Phys. Rev. B **106**, 115146 (2022).

[26] R. Pocha, D. Johrendt, B. Ni, and M. M. Abd-Elmeguid, Crystal structures, electronic properties, and pressure-induced superconductivity of the tetrahedral cluster compounds $GaNb_4S_8$, $GaNb_4Se_8$, and $GaTa_4Se_8$, J. Am. Chem. Soc. **127**, 8732 (2005).

[27] G. M. Sheldrick, A short history of *SHELX*, Acta Crystallogr. Sect. A: Found. Crystallogr. **64**, 112 (2008).

[28] O. V. Dolomanov, L. J. Bourhis, R. J. Gildea, J. A. K. Howard, and H. Puschmann, *OLEX*2: A complete structure solution, refinement and analysis program, J. Appl. Crystallogr. **42**, 339 (2009).

[29] See Supplemental Material at http://link.aps.org/supplemental/10.1103/PhysRevB.109.144101 for detailed information.

[30] C. Capillas, E. Kroumova, M. I. Aroyo, J. M. Perez-Mato, H. T. Stokes, and D. M. Hatch, *SYMMODES*: A software package for group-theoretical analysis of structural phase transitions, J. Appl. Crystallogr. **36**, 953 (2003).

[31] D. Orobengoa, C. Capillas, M. I. Aroyo, and J. M. Perez-Mato, *AMPLIMODES*: Symmetry-mode analysis on the Bilbao crystallographic server, J. Appl. Crystallogr. **42**, 820 (2009).

[32] J. M. Perez-Mato, D. Orobengoa, and M. I. Aroyo, Mode crystallography of distorted structures, Acta Crystallogr. Sect. A **66**, 558 (2010).

[33] D. Porter and C. Prestipino, Diffraction: Version 3.0.0, doi:10.5281/zenodo.8106031 (2023).

[34] C. S. Yadav, A. K. Nigam, and A. K. Rastogi, Thermodynamic properties of ferromagnetic Mott-insulator GaV_4S_8, Phys. B: Condens. Matter **403**, 1474 (2008).

[35] E. Ruff, S. Widmann, P. Lunkenheimer, V. Tsurkan, S. Bordács, I. Kézsmárki, and A. Loidl, Multiferroicity and skyrmions carrying electric polarization in GaV_4S_8, Sci. Adv. **1**, e1500916 (2015).

[36] M. M. Abd-Elmeguid, B. Ni, D. I. Khomskii, R. Pocha, D. Johrendt, X. Wang, and K. Syassen, Transition from Mott insulator to superconductor in $GaNb_4S_8$ and $GaTa_4Se_8$ under high pressure, Phys. Rev. Lett. **93**, 126403 (2004).

[37] V. Ta Phuoc, C. Vaju, B. Corraze, R. Sopracase, A. Perucchi, C. Marini, P. Postorino, M. Chligui, S. Lupi, E. Janod, and L. Cario, Optical conductivity measurements of $GaTa_4Se_8$ under high pressure: Evidence of a bandwidth-controlled insulator-to-metal Mott transition, Phys. Rev. Lett. **110**, 037401 (2013).